Electron-hole recombination via plasmon emission in narrow-gap semiconductors

A. Elci*

Department of Physics, North Texas State University, Denton, Texas 76203 [†]
(Received 16 August 1977)

When the plasma frequency coincides with the band gap in a narrow-gap semiconductor like $(Pb_{1-x}Sn_x)Se$, the electron-hole recombination is quite fast, in the picosecond range. Plasmon lifetime is calculated and taken into account in the calculation of the recombination rate. Experiments in which the plasmon-assisted recombination may be observed directly are proposed.

I. INTRODUCTION

Recent picosecond optical pulse measurements on Ge have shown that plasmons play a significant role in the nonlinear transmission of intense optical pulses. The optical properties of a Ge wafer irradiated by an intense Nd:glass laser pulse are significantly altered by the rapid recombinations of electrons and holes via plasmon emissions at high plasma densities. Due to these recombinations, nonlinear light absorption in Ge is observed to decrease relatively slowly and saturate at a higher absorption level as optical pulse energy is increased than otherwise would be expected. The dense plasmas created by the picosecond optical pulses display other properties that are also attributed to the plasmon-assisted electron-hole recombination.[1,2]

However, in all these measurements this type of recombination is observed only indirectly, since other equally rapid processes are taking place simultaneously while the energetic optical pulse is being absorbed in Ge. It would be desirable to observe the electron-hole recombination via plasmon emission more directly. The best materials in which this recombination can be more directly investigated are the narrow-gap semiconductor alloys $(Pb_{1-x}Sn_x)Se$, $(Pb_{1-x}Sn_x)Te$, and $(Cd_{1-x}Hg)Te$. In these materials, the energy gap E_G between conduction and valence bands is direct and can be continuously varied through zero by changing alloy composition or by applying hydrostatic pressure or magnetic field.[3-7] Some time ago, Wolff[8,9] suggested that it may be possible to induce plasma-wave instability in these materials by adjusting E_G to coincide with the plasma frequency $\hbar\omega_p$, then pumping holes or electrons into the semiconductor by an electron or laser beam. Whether or not stimulated plasmon emission occurs when electrons or holes are externally pumped, *there is an enhancement of electron-hole recombination if $E_G \sim \hbar\omega_p$*. If $E_G \sim \hbar\omega_p$, the pumped electrons and holes recombine via plasmon emission at a rate two to three orders of magnitude larger than the

rate at which they recombine via photon emission.[10] Plasmons which are emitted by the recombining electron-hole pairs generally have long wavelength ($\sim$ approximately sample dimension).

To illustrate the physics of the situation, let us consider a specific semiconductor $(Pb_{1-x}Sn_x)Se$. Its band structure is schematically shown in Fig. 1. The band gap is at L, and there are four conduction-band valleys.[11] Let us assume that temperature is low and that the conduction band is filled up to the Fermi level E_F which is considerably larger than E_G. A typical conduction-band electron density is $n_c \sim 10^{18}$ cm^{-3}. Now let us suppose that the semiconductor is pumped either optically (quanta of energy $h\nu_L$) or with an electron beam and a small density of holes (10^{14}–10^{15} cm^{-3}) is created. The thermalization rate for holes is relatively short[9] ($\lesssim 10^{-13}$ sec). Therefore holes rapidly lose energy and collect near the band edge as shown in Fig. 2. The hole Fermi level δE_p is assumed to be small; $\delta E_p \ll E_G$. Holes and electrons which are near the band edge begin to recombine. This recombination can occur through many mechanisms, which are discussed in detail in a review paper by Bonch-Bruevich and
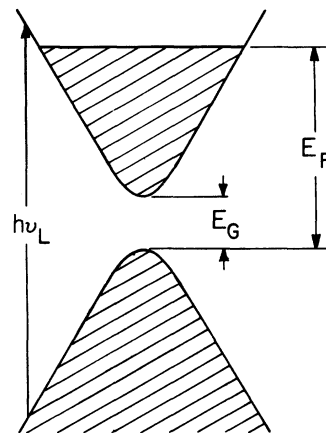

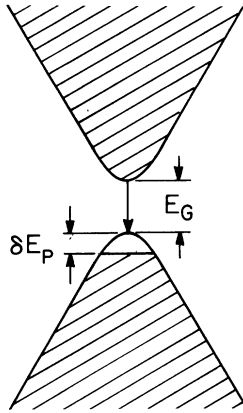FIG. 1. $(Pb_{1-x}Sn_x)$ Se band structure.

FIG. 2. Thermalized hole distribution.

Landsberg.[10] The special feature of the semi-conductors mentioned above is that when $E_G \sim \hbar \omega_p$, plasmon emission is exceedingly rapid and electron-hole recombination is therefore essentially determined by plasmon mechanism alone. It is the long-range portion of the electronic Coulomb field which induces the rapid recombinations in these materials.

In Wolff's original work on the plasma-wave instability,[9] the plasmon lifetime was taken as infinite in his calculation of the spontaneous plasmon-assisted recombination rate. Therefore the rate he obtained goes to zero for $\hbar \omega_p \leq E_G$. However plasmon decay in the semiconductor alloys mentioned above is rapid even for plasmons which have long wavelengths. The enhanced recombination can actually occur for band gaps larger than $\hbar \omega_p$ as a result of the short lifetime of plasmons and the consequent broadening of their energy.

In this paper, the spontaneous recombination rate of holes in an n-type narrow-gap semiconductor is calculated for finite plasmon lifetime. The plasmon lifetime is calculated in Sec. III, and found to be about 1 psec. The calculated recombination rate turns out to be quite large for a relatively wide interval of band gap values (see Fig. 5). Although the plasmon-assisted recombination rate is somewhat reduced for $E_G \gtrsim \hbar \omega_p$ compared to that for $E_G < \hbar \omega_p$, it is still considerably larger than the rates for other recombination mechanisms. For example, it is about two orders of magnitude larger than the rate of optical recombinations. In Sec. IV, experiments in which the plasmon-assisted recombination can be directly observed are suggested and discussed in some detail.

II. SPONTANEOUS RECOMBINATION RATE OF HOLES

In this section, the spontaneous recombination rate of holes is calculated for the carrier distri-

butions illustrated in Fig. 2. In the following calculation we make use of the propagator for plasmons and the self-energy method,[12-14] which are well known and will not be elaborated upon here. Let us note that the plasmon lifetime, or more precisely, the width of the plasmon resonance, which is $\hbar \times$ (plasmon lifetime)$^{-1}$, enters into the recombination rate calculation quite naturally when the self-energy method is used. In this section the plasmon resonance width is treated as an unknown parameter. It is evaluated in Sec. III.

Figure 3 shows the diagram for the recombination via plasmon emission. For a hole of wave vector $\vec{k}$, the recombination rate is given by[9]

$$\frac{1}{\tau_R(\vec{k})} = 2 \int \frac{d\vec{q}}{(2\pi)^3} \left[\frac{4\pi e^2 \hbar}{q^2 \epsilon_\infty} \right] \left[\frac{\vec{q} \cdot \vec{P}_{cv}}{m E_G} \right]^2$$

$$\times \mathrm{Im} \left[\frac{1}{\epsilon(\vec{q}, E_c(\vec{k}+\vec{q}) - E_v(\vec{k}))} \right] \quad (1)$$

Here m is the bare electron mass; $\vec{P}_{cv}$ is the interband matrix element of the momentum operator; and E_c and E_v are electron and hole energies, respectively. ϵ_∞ is the high frequency dielectric constant, and $\epsilon_\infty \epsilon(\vec{q}, \omega)$ is the overall dielectric function.[8] Note that

$$\lim_{\omega \to \infty} \epsilon(q, \omega) = 1 . \quad (2)$$

The $\vec{P}_{cv}$ factor in Eq. (1) comes from the interband matrix element of the density fluctuation operator, which, for long-wavelength fluctuations, is given by[15]

$$\langle c\vec{k} | e^{i\vec{q} \cdot \vec{r}} | v\vec{k}' \rangle \simeq -(\vec{q} \cdot \vec{P}_{cv} / m E_G) \delta^3(\vec{k}' + \vec{q} - \vec{k}) . \quad (3)$$

For the energy bands of $(Pb_{1-x} Sn_x)Se$, one can use the two-band model.[16] Then

$$E_c(\vec{k}) = \frac{E_G}{2} + \left[\left(\frac{E_G}{2} \right)^2 + E_G \frac{\hbar^2 \vec{k}^2}{2 m_{BE}} \right]^{1/2} , \quad (4a)$$

$$E_v(\vec{k}) = \frac{E_G}{2} - \left[\left(\frac{E_G}{2} \right)^2 + E_G \frac{\hbar^2 \vec{k}^2}{2 m_{BE}} \right]^{1/2} . \quad (4b)$$

m_{BE} is the effective mass at the band edge

$$\frac{1}{m_{BE}} = \left(\frac{1}{\hbar^2 k} \frac{dE_c(k)}{dk} \right)_{k=0} . \quad (5)$$
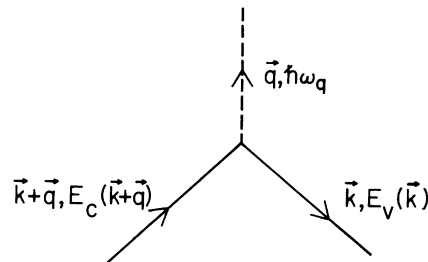

FIG. 3. Plasmon emission.

It is related to $\vec{P}_{cv}$ by the equation

$$1/m_{BE} = 2|\vec{P}_{cv}|^2/3m^2 E_G . \qquad (6)$$

Near the plasmon pole, Eq. (1) becomes

$$\frac{1}{\tau_R(\vec{k})} = \frac{e^2\hbar^2}{4\pi^2\epsilon_\infty}$$

$$\times \int d\vec{q} \left| \frac{\hat{q}\cdot\vec{P}_{cv}}{mE_G} \right|^2$$

$$\times \omega_q \left(\frac{\Delta(\vec{q})}{[\hbar\omega_q - E_c(\vec{k}+\vec{q}) + E_v(\vec{k})]^2 + [\frac{1}{2}\Delta(\vec{q})]^2} \right) ,$$

$$\qquad (7)$$

where $\hbar\Delta(\vec{q})^{-1}$ is the lifetime and ω_q is the frequency for a plasmon of wave vector $\vec{q}$. It is clear from (7) that when $E_G \sim \hbar\omega_p$, where ω_p is the plasma frequency for $q=0$, the resonance is set at $k \sim 0$ and $q \sim 0$. The hole densities we have in mind are small, and holes are confined to a small region near the band edge. Let us therefore set $\vec{k} = 0$. Near the pole, $\Delta(\vec{q})$ can be approximated by $\Delta(0)$ and thus treated as constant. We will also neglect plasmon dispersion and set $\omega_q = \omega_p$. ω_p is given by

$$\omega_p = (4\pi e^2 n_c/\epsilon_\infty m_{\Gamma S})^{1/2} , \qquad (8)$$

where n_c is the density of electrons in the conduction band and $m_{\Gamma S}$ is the effective mass at the Fermi surface

$$\frac{1}{m_{\Gamma S}} = \left(\frac{1}{\hbar^2 k} \frac{dE_c(k)}{dk} \right)_{k=k_F} . \qquad (9)$$

The hole-density contribution to the plasma frequency is neglected since the hole density is assumed to be small ($\sim 10^{14}$–10^{15} cm^{-3}, compared to $n_c \sim 10^{18}$ cm^{-3}).

Finally, for small $\vec{q}$, we can approximate (4a) by

$$E_c(\vec{q}) = E_G + \hbar^2\vec{q}^2/2m_{BE} . \qquad (10)$$

Thus the recombination rate in Eq. (7) becomes, at $\vec{k} = 0$,

$$\frac{1}{\tau_R(0)} = \frac{\hbar^2 e^2 \omega_p}{4\pi^2\epsilon_\infty}$$

$$\times \int d\vec{q} \left(\frac{\hat{q}\cdot\vec{P}_{cv}}{mE_G} \right)^2$$

$$\times \frac{\Delta(0)}{(\hbar\omega_p - E_G - \hbar^2 q^2/2m_{BE})^2 + [\frac{1}{2}\Delta(0)]^2} .$$

$$\qquad (11)$$

This integral can be evaluated analytically. If we define

$$\rho \equiv E_G/\hbar\omega_p \qquad (12)$$

and

$$\zeta \equiv \Delta(0)/2\hbar\omega_p , \qquad (13)$$

then Eq. (11) becomes

$$\frac{1}{\tau_R(0)} = \left(\frac{6^{1/2} e^2 \omega_p m\zeta}{\hbar\epsilon_\infty |\vec{P}_{cv}|} \right)$$

$$\times \{\rho[(\rho-1)^2 + \zeta^2]^{1/2} + \rho(\rho-1)\}^{-1/2} . \qquad (14)$$

Note that as the plasmon width $\Delta(0)$ goes to zero,

$$\lim_{\zeta\to 0} \zeta\{\rho[(\rho-1)^2 + \zeta^2]^{1/2} + \rho(\rho-1)\}^{-1/2}$$

$$= \begin{cases} 0 & \text{for } \rho > 1 , \\ 2^{1/2}\rho^{-1/2}(1-\rho)^{1/2} & \text{for } \rho < 1, \end{cases}$$

and (14) reduces to the expression given by Wolff[9] (neglecting δE_p, the hole Fermi energy).

III. PLASMON LIFETIME

In order to complete the calculation of the spontaneous recombination rate, we need the plasmon resonance width for long-wavelength plasmons, i.e., $\Delta(0)$. Here, we calculate the plasmon decay for the lowest-order perturbation diagrams, since higher-order diagrams are not expected to contribute to the decay in any significant amount. We have only indicated the outlines of the calculation in the text. The details are discussed in the Appendix.

$(Pb_{1-x}Sn_x)Se$, $(Pb_{1-x}Sn_x)Te$, and $(Cd_{1-x}Hg_x)Te$ are relatively degenerate when $\hbar\omega_p \sim E_G$, for both n-type and p-type samples. Long-wavelength plasmons decay primarily via impurity scattering in these materials. As the plasmon wavevector $q \to 0$, other plasmon decay mechanisms—e.g., Landau damping and phonon scattering—are rela-
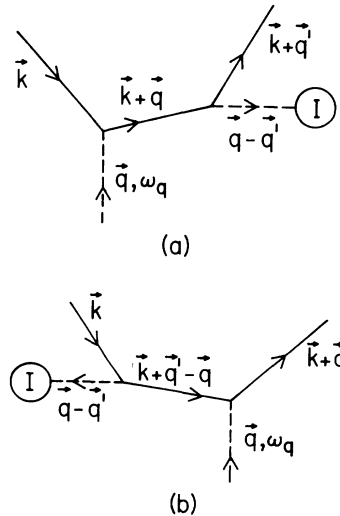

FIG. 4. Plasmon-impurity scattering.

tively unimportant,[17] and will be ignored in this paper.

The lowest order plasmon-impurity scattering is shown in Figs. 4(a) and 4(b). Here a plasmon breaks up into an electron and a hole in the fixed field of the impurity. The impurity imparts enough momentum to the incoming plasmon to permit the transfer of the plasmon energy to individual particle states, i.e., to raising an electron above the Fermi level, leaving an empty state behind, in the conduction band. Since the impurity is fixed in space, no energy is given to or taken from it. As the initial plasmon momentum goes to zero, the contribution of these diagrams remains constant and large.

The net amplitude for the plasmon decay in a screened impurity field is the sum of the two diagrams shown in Fig. 4 (Ref. 18):

$$i\left(\frac{4\pi e^2 \hbar^2 \omega_q}{q^2 \epsilon_\infty}\right)^{1/2}\left(\frac{4\pi e^2}{\epsilon_\infty}\right)\left(\frac{1}{|\vec{q}-\vec{q}'|^2+\kappa^2}\right)\sum_{i=1}^{n_i} e^{-i(\vec{q}-\vec{q}')\cdot\vec{R}_i}\left(\frac{1}{\hbar\omega_q - E_c(\vec{k}+\vec{q})+E_c(\vec{k})}\right.$$

$$\left.-\frac{1}{\hbar\omega_q - E_c(\vec{k}+\vec{q}')+E_c(\vec{k}+\vec{q}'-\vec{q})}\right),$$

where $\vec{k}$, $\vec{q}$, and $\vec{q}'$ are as defined in the diagrams, R_i refers to the position of an impurity, n_i is the number of impurities in the volume (which is taken to be unity in the calculation), and κ is the Fermi-Thomas wave vector

$$\kappa^2 = 3\omega_p^2/v_F^2 = 3\omega_p^2 m_{\text{FS}}^2/\hbar^2 k_F^2 . \tag{15}$$

The absolute square of this amplitude contains the factor

$$\sum_{i=1}^{n_i}\sum_{j=1}^{n_i} e^{-i(\vec{q}-\vec{q}')\cdot(\vec{R}_i-\vec{R}_j)} .$$

Impurities are distributed randomly and therefore to a good approximation we may take the sum of the diagonal terms $(i=j)$ alone,[19] which gives n_i. Let us define the partial width

$$\Gamma(\vec{q}, \vec{q}', \vec{k}) = \left(\frac{2\pi}{\hbar}\right)n_i\left(\frac{2\pi e^2 \hbar^2 \omega_q}{q^2 \epsilon_\infty}\right)\left(\frac{4\pi e^2}{\epsilon_\infty}\right)^2\left(\frac{1}{|\vec{q}-\vec{q}'|^2+\kappa^2}\right)^2$$

$$\times\left(\frac{1}{\hbar\omega_q - E_c(\vec{k}+\vec{q})+E_c(\vec{k})} - \frac{1}{\hbar\omega_q - E_c(\vec{k}+\vec{q}')+E_c(\vec{k}+\vec{q}'-\vec{q})}\right)^2 \delta(E_c(\vec{k}+\vec{q}')-E_c(\vec{k})+\hbar\omega_q). \tag{16}$$

Integrating over all possible final states with appropriate weighting factors, we then obtain the plasmon resonance width at the plasmon wave vector $\vec{q}$:

$$\Delta(\vec{q}) = \int\frac{2d\vec{k}}{(2\pi)^3}\int\frac{d\vec{q}'}{(2\pi)^3} \Gamma(\vec{q},\vec{q}', \vec{k})f_{\vec{k}}^c(1 - f_{\vec{k}+\vec{q}'}^c), \tag{17}$$

where $f_{\vec{k}}^c$ is the Fermi function for electrons with a temperature $T = (k_B\beta)^{-1}$,

$$f_{\vec{k}}^c = 1/(e^{\beta[E_c(k)-E_F]} +1) . \tag{18}$$

The integrals in Eq. (17) are evaluated in the Appendix for $q \to 0$ and $T \to 0$. Within the approximations indicated there, Eq. (17) for $\vec{q}=0$ is

$$\Delta(0) \simeq \Delta_0\left\{\frac{32\xi^4 + 72\xi^2 + 30 - 6\lambda^2\xi^2(5+2\xi^2)}{3\xi^2(1+\xi^2)} + (2+\lambda^3)\ln\left(\frac{1+\xi^2(1+\lambda)^2}{1+\xi^2(1-\lambda)^2}\right) + 3\lambda^2\ln[1+2\xi^2(\lambda^2+1)+\xi^4(\lambda^2-1)^2]\right.$$

$$\left.-\frac{1}{\xi}\left(\frac{5}{\xi^2}+9\right)[\tan^{-1}(\xi\lambda+\xi)-\tan^{-1}(\xi\lambda-\xi)]\right\}, \tag{19}$$

where the parameters are

$$\Delta_0 \equiv e^4 m^4 \omega_p^2 n_i/12\pi e_\infty^2 m_{\text{FS}}|\vec{P}_{cv}|^4 n_c , \tag{20}$$

$$\xi \equiv m\hbar k_F/m_{\text{FS}}|\vec{P}_{cv}| , \tag{21}$$

and

$$\lambda \equiv (2E_F - E_G)/\hbar\omega_p. \tag{22}$$

To get some feeling for the actual numbers involved in these calculations, let us consider a sample of $(Pb_{1-x}Sn_x)Se$ for which $x \sim 0.18$ and therefor $E_G \sim 0.03$ eV.[5] For these alloys, $\epsilon_\infty \sim 20$. Rabii's measurements on PbSe give[20]

$$\hbar^2 |\vec{P}_{cv}|^2/3m^2 \simeq 1.85 \times 10^{-39} \text{ erg}^2 \text{ cm}^2. \tag{23}$$

Let $n_c = 10^{18}$ cm^{-3}. In the limit of degenerate carriers

$$k_F = (\tfrac{3}{4}\pi^2 n_c)^{1/3} \simeq 2 \times 10^6 \text{ cm}^{-1}. \tag{24}$$

From (4a) and (6) one finds

$$E_F = \frac{E_G}{2} + \left[\left(\frac{E_G}{2}\right)^2 + \frac{\hbar^2 |\vec{P}_{cv}|^2}{3m^2} k_F^2\right]^{1/2}. \tag{25}$$

When $E_G \sim 0.03$ eV, the last term under the radical sign is an order of magnitude larger than the first one.[21] Neglecting the latter, (25) can be approximated by

$$E_F = \frac{E_G}{2} + \frac{\hbar k_F |\vec{P}_{cv}|}{m\sqrt{3}} \simeq \frac{E_G}{2} + 0.058 \text{ eV}. \tag{26}$$

Using (26), one then finds that

$$m_{FS}/m \simeq \sqrt{3}\, \hbar k_F/|\vec{P}_{cv}| \simeq 4.5 \times 10^{-2}, \tag{27a}$$

$$\xi \simeq 1/\sqrt{3}, \tag{27b}$$

$$\hbar\omega_p = \hbar(4\pi e^2 n_c/\epsilon_\infty m_{FS})^{1/2} \simeq 0.034 \text{ eV}, \tag{27c}$$

and

$$\lambda \simeq 2k_F |\vec{P}_{cv}|/\omega_p m\sqrt{3} \simeq 3.0. \tag{27d}$$

Therefore $\Delta(0)$ is independent of E_G as long as (26) is valid. Setting $n_i \simeq n_c$, we find $\Delta_0 \simeq 2 \times 10^{-5}$ eV and $\Delta(0) \simeq 10^{-3}$ eV. Thus, the lifetime of long-wavelength plasmons is about 1 psec.

The recombination rate versus $\rho = E_G/\hbar\omega_p$ for $\Delta(0) \simeq 10^{-3}$ eV is plotted in Fig. 5. It is seen that electron-hole recombination is enhanced and extremely rapid even for $E_G > \hbar\omega_p$. It is also seen that the recombination rate varies as $\Delta(0)\rho^{-1/2}(\rho - 1)^{-1/2}$ for $\rho > 1$. This portion of the curve arises entirely from the finite plasmon lifetime.

It might be possible to reproduce this theoretical curve experimentally. The rapidity of the recombination might also be of some use in new devices. We now turn our attention to this subject.

IV. EXPERIMENTAL OBSERVATION AND DISCUSSION

For the sake of definiteness, we will continue to refer to a specific n-type $(Pb_{1-x}Sn_x)Se$ sample. However, only a slight modification of the theoretical discussion offered here applies equally well to p-type $(Pb_{1-x}Sn_x)Se$, and to both n- and p-type $(Pb_{1-x}Sn_x)Te$ and $(Cd_{1-x}Hg_x)Te$.

One direct method of studying the enhanced recombination is to do a reflectivity experiment. Optical pulses of extremely short duration (a few picoseconds) can be achieved by mode-locked lasers.[22] These pulses can be used to measure the decay in the density of electrons and holes which are pumped optically. The schematic of such an experiment is shown in Fig. 6. The sample is assumed to be thin, $W \sim 1$ μm. The optical pulse from the second harmonic of a CO_2 laser creates the holes. For the second harmonic of the CO_2 laser, $h\nu_L = 0.234$ eV $> 2E_F - E_G$, and the light absorption coefficient of the semiconductor at this frequency is $\alpha(\nu_L) \sim 10^4$ cm^{-1}. Another pulse, from the first harmonic of the CO_2 laser $[h\nu = 0.117$ eV

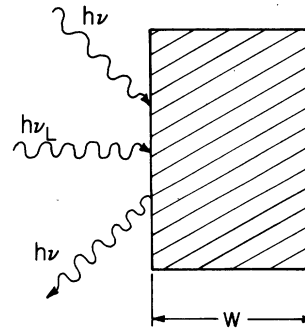FIG. 5. Plasmon-assisted recombination rate; $\rho \equiv E_G/\hbar\omega_p$.

Plot labels: $\hbar\omega_P = 0.034$ eV, $\Delta(0) = 0.001$ eV. Vertical axis: RECOMBINATION RATE (sec^{-1}) from 10^{11} to 10^{13}. Horizontal axis: ρ from 0.80 to 2.00.

FIG. 6. Schematic of reflectivity experiment.
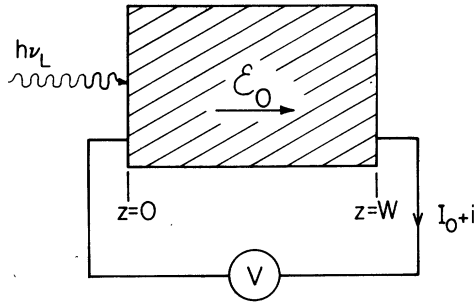
FIG. 7. Schematic of photoconductivity experiment.

FIG. 8. Hole distribution in constant electric field.

$\lesssim 2E_F - E_G$; $\alpha(\nu) < \alpha(\nu_L)]$, is incident on the sample (normal or at an angle), but is delayed compared to the first pulse. The reflectivity of the second pulse can be measured and related to the hole density created by the first. The time interval between the two pulses can be varied to observe the decrease in the hole density at different delay times. For thin samples $(W \sim \alpha^{-1})$, the decay in the hole density is entirely due to recombinations[23]

$$n_h \propto \exp(-t_{\text{delay}}/\tau_R) . \tag{28}$$

Such thin samples can be grown epitaxially. In such an experiment, hydrostatic pressure can be applied to the sample by putting it into a diamond cell. Since E_G varies with hydrostatic pressure $(dE_G/dP = -8.65 \times 10^{-6}$ eV/bar),[24] $1/\tau_R$ can be mapped experimentally as a function of E_G.

The proposed experiment is quite similar in technical detail to those discussed in Refs. 1, 2, and 25. For more information on experimental technique, the reader is referred to these papers and to the references cited therein.

Although the recombination rate is rapid, it is possible to do a photoconductivity experiment to measure it. Since such an experiment allows $1/\tau_R$ to be varied without changing E_G, we will discuss it in some detail. The schematic of the experiment is shown in Fig. 7. A thin wafer of thickness W is subjected to a drift field $\vec{\mathcal{S}}_0$. There is a current I_0 flowing through the sample. An optical beam, e.g., from a cw CO laser, is turned on and creates holes. Holes thermalize and collect, not, however, at the band edge as discussed previously, but at a region below the band edge because of the drift induced by the constant electric field.[26] This is illustrated in Fig. 8. The shift of the hole distribution from the top of the valence band is, approximately,

$$\Delta E = \tfrac{1}{2} m_{\text{BE}} (\mu_h \mathcal{S}_0)^2 , \tag{29}$$

where μ_h is the hole mobility. The expression for the recombination rate given in (14) can still be used if E_G in ρ is replaced by an effective gap
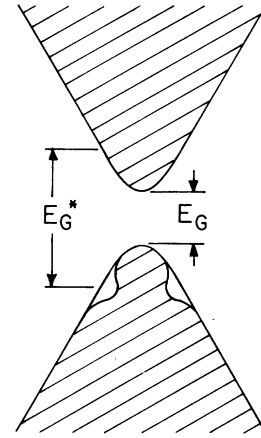
$$E_G^* = E_G + 2\Delta E . \tag{30}$$

Thus the recombination rate is dependent on the electric field applied. The recombination rate can therefore be changed by varying the electric field, as well as by varying the band gap.

When the laser beam is on, holes are generated near $z = 0$. Holes drift and diffuse in the direction of the electric field; many of them recombine. But if the sample thickness is small and the applied electric field large, then there is a sufficient number of holes reaching the surface at $z = W$ to give an appreciable photoinduced current. The photoinduced hole current density is given by

$$j_h = e \mu_h \mathcal{S}_0 n_h - e D_h \frac{dn_h}{dz} , \tag{31}$$

where n_h is the photogenerated hole density and D_h is the hole diffusion constant. In steady state,

$$\frac{1}{e} \frac{d}{dz} j_h + \frac{n_h}{\tau_R} \simeq G\delta(z) , \tag{32a}$$

where $G = $ (light speed) $\times$ (the number of photons per unit volume in the light beam). Since the photogenerated holes are extracted at $z = W$,

$$n_h(W) = 0 . \tag{32b}$$

The solution of (32a) and (32b) is given by

$$n_h(z) = 2G \left[\exp\left(\frac{\mu_h \mathcal{S}_0 z}{2D_h} \right) \right] \sinh\left(\frac{W-z}{l_h} \right)$$

$$\times \left[\mu_h \mathcal{S}_0 \sinh\left(\frac{W}{l_h} \right) + 2D_h l_h \cosh\left(\frac{W}{l_h} \right) \right]^{-1} , \tag{33a}$$

where

$$l_h \equiv \left[\left(\frac{\mu_h \mathcal{S}_0}{2D_h} \right)^2 + \frac{1}{D_h \tau_R} \right]^{-1/2} . \tag{33b}$$

Thus the current density is at $z = W$,

$$j_h(z = W) = \left(\frac{2eGD_h}{l_h} \right) \exp \left(\frac{\mu_h \mathcal{E}_0 W}{2D_h} \right)$$

$$\times \left[\mu_h \mathcal{E}_0 \sinh \left(\frac{W}{l_h} \right) \right.$$

$$\left. + 2D_h l_h \cosh \left(\frac{W}{l_h} \right) \right]^{-1} . \qquad (34)$$

For $(Pb_{1-x} Sn_x)Se$ alloys, $\mu_h \sim 10^4$ cm^2/V sec and $D_h \sim 2 \times 10^2$ cm^2/sec. If $\tau_R = 10^{-11}$ sec, $W = 10$ μm, and $\mathcal{E}_0 = 3 \times 10^3$ V/cm, and if the power delivered by the laser is designated P_L, then the current is

$$i_h = A j_h(W) = 500 P_L \text{ mA} , \qquad (35)$$

where P_L is measured in watts. [A is the area on which the light beam is focused; i_h is independent of A for the boundary condition (32b)]. Thus, even at modest cw laser power outputs, the photoin-duced currents will be measurable. From con-ductivity measurements one can then determine τ_R (via l_h) as a function of the applied electric field. The role of the electric field is twofold: it induces carrier drift, and it changes τ_R via the effective gap.

Although we have concentrated on the experi-mental arrangement illustrated in Fig. 7, an ex-perimentally better geometry is probably the one illustrated in Fig. 9, since the light beam falls on an area adjacent to the current probe and since the optical alignment can be adjusted to obtain the maximum photoinduced currents for a given laser output and applied field.

One might worry that in the suggested experi-ments the semiconductor would begin to lase due to the inverted electron-hole population and that this would interfere with the plasmon-assisted re-combination. This need not be a problem. When the hole densities are in the range 10^{14}–10^{15} cm^{-3}, the semiconductor alloys we have been discussing

lase only at quite low temperatures. The proposed experiments can be done at liquid-nitrogen or room temperature.

Plasmon-assisted electron-hole recombinations can be used in modulating the density-dependent parameters of the narrow-gap semiconductors. Nurmikko and Pratt suggested an application of this to modulate infrared radiation in picosecond range[27] which is of some practical interest. The light-absorption coefficient $\alpha(\nu)$ of a direct gap crystal is a relatively sensitive function of the carrier densities. If a large number of carriers are created by an intense light beam, $\alpha(\nu)$ de-creases and the crystal becomes transparent. Transparency may increase by as much as three to five times, depending upon the pulse intensity. After the pulse, recombinations reduce the car-rier density and eventually restore $\alpha(\nu)$ to its original value. For $(Pb_{1-x} Sn_x)Se$ and $(Pb_{1-x} Sn_x)Te$ crystals, the intense excitation pulses can have ν near the visible end of the spectrum. If $E_G \sim \hbar \omega_p$, these pulses produce picosecond trans-ients in $\alpha(\nu)$ due to the fast recombinations. Therefore, if a light signal whose frequency is near the absorption edge ($h\nu \sim E_G$, which is far infrared) is sent through the sample as it is being pulsed by short-wavelength radiation, the trans-mitted infrared signal will be modulated in pico-second range. Nurmikko and Pratt appear to have observed these transients.

In summary, we have shown that in narrow-gap semiconductors the plasmon-assisted recombina-tion is extremely rapid if the band gap and the plasma frequency are close. We have calculated the recombination rate and suggested experiments in which this type of recombination can be investi-gated. We have discussed its behavior in a constant electric field. We have also discussed a particular case in which the rapidity of the recombination might be usefully applied to devices.

FIG. 9. Schematic of a photoconductivity experiment.

APPENDIX

In this Appendix, the integral involved in Eq. (17) is evaluated in the long-wavelength approximation at zero temperature. The purpose of the Appendix is essentially to illustrate the approximations in-volved in arriving at Eq. (19).

As plasmons decay, electronic transitions occur across the Fermi surface; therefore, for $q \to 0$, the energy denominators in Eq. (16) become

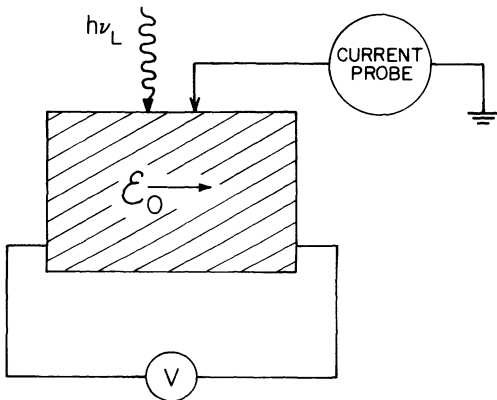$$\frac{1}{\hbar\omega_q - E_c(\vec{k}+\vec{q}) + E_c(\vec{k})} - \frac{1}{\hbar\omega_q - E_c(\vec{k}+\vec{q}') + E_c(\vec{k}+\vec{q}'-\vec{q})} \simeq -\frac{1}{(\hbar\omega_p)^2}\,\vec{q}\cdot[\nabla_{\vec{k}}E_c(\vec{k}+\vec{q}') - \nabla_{\vec{k}}E_c(\vec{k})]$$

$$\simeq -\frac{1}{(\hbar\omega_p)^2}\,\vec{q}\cdot\vec{q}'\left(\frac{1}{k}\frac{dE_c(\vec{k})}{dk}\right)_{k=k_F} = \frac{-\vec{q}\cdot\vec{q}'}{m_{FS}\,\omega_p^2}\ . \qquad (A1)$$

Thus Eq. (17) for $\vec{q}=0$ becomes

$$\Delta(0) = \left(\frac{\hbar e^4 n_i}{6\pi^3\epsilon_\infty^2 m_{FS} n_c \omega_p}\right)\int d\vec{k}\int d\vec{q}'\,\frac{(q')^2}{[(q')^2+\kappa^2]^2}\,f_{\vec{k}}^c(1-f_{\vec{k}+\vec{q}'}^c)\delta(E_c(\vec{k}+\vec{q}') - E_c(\vec{k}) - \hbar\omega_p)\ . \qquad (A2)$$

Because of the δ function and (18), in the limit of zero temperature

$$f_{\vec{k}}^c(1-f_{\vec{k}+\vec{q}'}^c)\delta(E_c(\vec{k}+\vec{q}') - E_c(\vec{k}) - \hbar\omega_p) = \frac{1}{1+e^{\beta[E_c(k)-E_F]}}$$

$$\times\left(1 - \frac{1}{1+e^{\beta[E_c(k)+\hbar\omega_p-E_F]}}\right)\delta(E_c(\vec{k}+\vec{q}') - E_c(\vec{k}) - \hbar\omega_p)$$

$$\xrightarrow{T\to 0}\begin{cases}\delta(E_c(\vec{k}+\vec{q}') - E_c(\vec{k}) - \hbar\omega_p) & \text{if } E_c(\vec{k}) \le E_F \le E_c(\vec{k}) + E_F, \\ 0 & \text{otherwise.}\end{cases} \qquad (A3)$$

Thus, when conduction electrons are degenerate, Eq. (17) can be written

$$\Delta(0) \simeq \frac{\hbar e^4 n_i}{6\pi^3\epsilon_\infty^2 m_{FS} n_c \omega_p}\int_{E_c(\vec{k})\le E_F \le E_c(\vec{k})+\hbar\omega_p} d\vec{k}\int d\vec{q}\,\frac{q^2\delta(E_c(\vec{k}+\vec{q}) - E_c(\vec{k}) - \hbar\omega_p)}{(q^2+\kappa^2)^2}\ , \qquad (A4)$$

where we have dropped the prime on $\vec{q}$. When $E_c(\vec{k})$ in (4a) is substituted into (A4), the $\vec{q}$ integral becomes

$$2\pi\int_0^\infty dq\,q^2\int_{-1}^{+1}d(\cos\theta)\,\frac{q^2}{(q^2+\kappa^2)^2}$$

$$\times\delta\left(\left[\left(\frac{E_G}{2}\right)^2+\frac{\hbar^2 E_G}{2m_{BF}}(k^2+q^2+2kq\cos\theta)\right]^{1/2} - \left[\left(\frac{E_G}{2}\right)^2+\frac{\hbar^2 E_G k^2}{2m_{BF}}\right]^{1/2} - \hbar\omega_p\right)$$

$$= \left(\frac{2\pi m_{BF}}{\hbar^2 E_G k}\right)[2E_c(k)+2\hbar\omega_p - E_G]\int_{Q_-(k)}^{Q_+(k)}dq\,\frac{q^3}{(q^2+\kappa^2)^2}\ , \qquad (A5)$$

where

$$Q_\pm(k) = \pm k + \{k^2 + (2m_{BF}\,\hbar\omega_p/\hbar E_G)[\hbar\omega_p - E_G + 2E_c(k)]\}^{1/2}\ . \qquad (A6)$$

The remaining integral in (A5) is elementary

$$\int_{Q_-(k)}^{Q_+(k)}dq\,\frac{q^3}{(q^2+\kappa^2)^2} = \frac{1}{2}\left[\frac{Q_-^2}{\kappa^2+Q_-^2} - \frac{Q_+^2}{\kappa^2+Q_+^2} + \ln\left(\frac{\kappa^2+Q_+^2}{\kappa^2+Q_-^2}\right)\right]\ . \qquad (A7)$$

To do the $\vec{k}$ integration, we note that the integrand does not depend on the direction of $\vec{k}$. Integration of the angular variables of $\vec{k}$ gives 4π. To evaluate the remaining integral, it is more convenient to change the integration variable from k to

$$E \equiv E_c(k) = \tfrac{1}{2}E_G + [(\tfrac{1}{2}E_G)^2 + \hbar^2 k^2 E_G/2m_{BF}]^{1/2}\ . \qquad (A8)$$

In terms of E, Eq. (A6) becomes

$$Q_\pm(E) = (2m_{BF}/\hbar^2 E_G)^{1/2}\{[(E+\hbar\omega_p)(E+\hbar\omega_p - E_G)]^{1/2} \pm [E(E-E_G)]^{1/2}\}\ . \qquad (A9)$$

Therefore Eq. (A4) becomes

$$\Delta(0) \simeq \left(\frac{2e^4 n_i m_{BF}^2}{3\pi\epsilon_\infty^2 m_{FS} n_c \omega_p\hbar^3 E_G^2}\right)\int_{E_F-\hbar\omega_p}^{E_F}dE(2E-E_G)(2E+2\hbar\omega_p - E_G)\left[\frac{Q_-^2}{\kappa^2+Q_-^2} - \frac{Q_+^2}{\kappa^2+Q_+^2} + \ln\left(\frac{\kappa^2+Q_+^2}{\kappa^2+Q_-^2}\right)\right]\ . \qquad (A10)$$

Note that E is confined to a thin shell at the Fermi surface: $E_F - \hbar\omega_p \leq E \leq E_F$. E is therefore large relative to E_G or $\hbar\omega_p$. Thus, to a good approximation, (A9) can be written

$$Q_+ \simeq (2m_{BE}/\hbar^2 E_G)^{1/2}(2E + \hbar\omega_p - E_G) , \qquad (A11)$$

$$Q_- \simeq (2m_{BE}/\hbar^2 E_G)^{1/2}(\hbar\omega_p) . \qquad (A12)$$

The logarithmic terms in (A10) can then be integrated by parts, and the other integrals are elementary. Integrating over E and substituting the value of m_{BE}/E_G and κ from (6) and (15), respectively, we obtain the expression given by (19).

---

†Visiting.

[1] A. Elci et al., Phys. Rev. B 16, 191 (1977).

[2] H. M. van Driel et al. (to be published).

[3] J. R. Dixon and R. F. Bis, Phys. Rev. 176, 942 (1972).

[4] J. O. Dimmock, I. Melngailis, and A. J. Strauss, Phys. Rev. Lett. 16, 1193 (1966).

[5] A. R. Calawa, J. O. Dimmock, T. C. Harman, and I. Melngailis, Phys.Rev. Lett. 23, 7 (1969).

[6] J. Stankiewicz and W. Giriat, Phys. Status Solidi B 49, 387 (1972).

[7] M. W. Scott, J. Appl. Phys. 40, 4077 (1969).

[8] P. A. Wolff, Phys. Rev. Lett. 24, 266 (1970).

[9] P. A. Wolff, in The Physics of Semimetals and Narrow Gap Semiconductors, edited by X. Carter and X. Bate (Pergamon, Oxford and New York, 1971).

[10] V. L. Bonch-Bruevich and E. G. Landsberg, Phys. Status Solidi 29, 9 (1968).

[11] $(Pb_{1-x}Sn_x)Te$ has six conduction-band valleys. $(Cd_{1-x}Hg_x)Te$ has just one, at Γ. However its valence bands are a little more complicated. It has two valence bands which are degenerate at Γ.

[12] D. F. Dubois, Ann. Phys. (N.Y.) 8, 24 (1959).

[13] J. J. Quinn, Phys. Rev. 126, 1453 (1962).

[14] D. Pines, The Many-Body Problem (Benjamin, New York, 1962).

[15] H. Ehrenreich and M. H. Cohen, Phys. Rev. 115, 786 (1959).

[16] P. A. Wolff, J. Phys. Chem. Solids 25, 1057 (1964). For $(Pb_{1-x}Sn_x)Se$ and $(Pb_{1-x}Sn_x)Te$, the constant energy surfaces in the $\vec{k}$ space are actually ellipsoids. For $(Pb_{1-x}Sn_x)Se$, the anistropy in the $\vec{k}$ space is not as important as for $(Pb_{1-x}Sn_x)Te$. The essential physics remains the same whether the anisotropy is included

in the calculation or not.

[17] For $q \to 0$, the Landau damping of plasmons $\sim q^{-1} \times \exp(-const/q^2) \to 0$. See, e.g., N. D. Mermin and E. Canal, Ann. Phys. (N.Y.) 26, 247 (1964); and V. Celli and N. D. Mermin, ibid. 30, 249 (1964). In a phonon scattering, phonons carry off a portion of the energy with which the electron may make the transition to an energy above the Fermi surface. This reduces the effectiveness of the phonon scattering for $q \to 0$.

[18] For impurity calculations, the reader is referred to J. R. Klauder, Ann. Phys. (N.Y.) 14, 43 (1961); and P. A. Wolff, Phys. Rev. 126, 405 (1962); see also Ref. 19.

[19] J. S. Langer, Phys. Rev. 120, 714 (1960).

[20] S. Rabii, Phys. Rev. 167, 801 (1968). Rabii's measurements actually give the transverse and longitudinal effective masses, m_t and m_l, respectively, at $E_G = 0.16$ eV. He finds that $m_t/m \simeq 0.06$ and $m_l/m \simeq 0.10$. Eq. (23) in the text is obtained from $1/m_{BE} = \frac{2}{3} 1/m_t + \frac{1}{3} 1/m_l$ and from Eq. (6) in the text.

[21] For $E_G = 0.03$ eV, $m_{BE}/m \simeq 10^{-2}$.

[22] D. von der Linde, Appl. Phys. 2, 281 (1973). With mode-locked lasers, hole densities much larger than 10^{15} cm^{-3} can be created if necessary.

[23] For thicker samples, one must take into account the diffusion of the photogenerated carriers from the region near the surface into the interior of the semiconductor.

[24] I. Melngailis, T. C. Harman, and J. A. Kafalas, Proceedings of the Conference on the Physics of IV-VI Compounds and Alloys, Philadelphia, 1972 (unpublished).

[25] D. H. Auston and C. V. Shank, Phys. Rev. Lett. 32, 1120 (1974).

[26] E. M. Conwell, in Solid State Physics, Suppl. 9 (Academic, New York, 1967).

[27] A. V. Nurmikko and G. W. Pratt, Jr. (private communication).